Estimation of numerical substrate properties with compartmentalized models from Monte-Carlo simulated DW-MRI signals

Remy Gardier[a,*], Juan Luis Villarreal Haro[a], Erick J Canales-Rodríguez[a], Gabriel Girard[a,b], Jonathan Rafael-Patino[a,b], Jean-Philippe Thiran[a,b,c]
a Signal Processing Laboratory (LTS5), Ecole Polytechnique Fédérale de Lausanne (EPFL), Lausanne, Switzerland
b Radiology Department, Centre Hospitalier Universitaire Vaudois and University of Lausanne, Lausanne, Switzerland
c CIBM Center for Biomedical Imaging, Switzerland
*Correspondence: Rémy Gardier, remy.gardier@epfl.ch

Synopsis
For over a decade, microstructure imaging has been a hot research topic in DW-MRI. Tissue complexity compelled researchers to make assumptions about certain properties. The inverse problem of microstructure imaging, in particular, is ill-posed, and current methods fix some parameters to reduce the solution space. In this abstract, we look at how intracellular and extracellular diffusion coefficients affect the estimation of compartmentalized model parameters. We show that robust estimation of some parameters does not extend to all parameters using Monte-Carlo simulations in impermeable substrates with multiple diffusivities, and we identified the extracellular compartment as the most influential on estimation quality.

Introduction
Monte-Carlo diffusion simulations (MCDS) showed promising results for realistic diffusion-weighted magnetic resonance imaging (DW-MRI) signal generation[1, 2]. In-silico experiments offer the opportunity to test and validate new models of tissue microstructure. In this work, we use MCDS to investigate the bias of parameters estimation of compartmentalized models when fixing the diffusion coefficient in substrates composed of a collection of spheres of gamma-distributed radii.

Methods
In this work, we used the three-compartment model VERDICT[3] designed for microstructure estimation of spherical cells. Among the parameters of the model, we estimated the intra-cellular (f_{in}), extra-cellular (f_{ex}) and the vascular (f_v) volume fractions, the average cell radius (R), and the intra-/extra-cellular diffusion coefficients (D_i, D_e) with the Levenberg-Marquardt (LM) optimization algorithm [4]. Because diffusion signals in our substrates were isotropic, the main direction of the vascular compartment was not relevant. We fixed the pseudo diffusion coefficient to 8 10^{-9} m^2/s [5] and constrained the sum of the volume fractions to one. We fitted the model with four different constraints on D_i and D_e for investigating their influence on the parameters' estimation. We fixed them in two cases, either to the *ground-truth* or to widely-used *fixed* values (0.5 and 2 10^{-9} m^2/s) [4, 5]. In the third and fourth cases, we estimated them with *coupled* and *unconstrained* equality. R, f_{in}, and f_{ex} were estimated during the optimization procedure. We simulated the DW-MRI signals with an extended version of the publicly available MCDC simulator [1], adapted to simulate diffusion in substrates with distinct intra and extra diffusion coefficients. Substrates were single-voxel cubes of side length 70 μm filled with spheres of radii sampled from a gamma distribution of mean 1.5 μm and variance 0.75 μm^2. We used four substrates having f_{in} from 0.3 to 0.6 (Fig.1). D_i and D_e were 1,2 or 3 10^{-9} m^2/s, and 0.1, 0.5 or 1 10^{-9} m^2/s, respectively. For all simulations, 3.5×10^5 particles were randomly initialized within the substrates and diffused during 50 ms. The time step was set to 5 μs, and the step length is calculated with $\delta sk=\sqrt{6Dk\delta t}$ for each compartment. DW-MRI signals were generated with a PGSE sequence with TE= 50 ms and δ= 4.5 ms in 24 directions for three b-shells(1, 2 and 4 $10^9 s/m^2$). Each signal was corrupted 30 times with Rician noise for three signal-to-noise ratios (SNR) (20, 50, and 100).

Results and discussion
The quality of the estimation of f_{in} and f_{ex} depends on D_e of the substrate mostly. For D_e = 0.1 10^{-9} m^2/s, f_{ex} is underestimated while f_{in} is overestimated for all pairs (D_i, D_e) and all methods (see Fig. 2 left column). Fig.3 shows the MAE on f_{in} that ranges from 0.05 for *ground-truth* to 0.5 for *fixed* method. As D_e increases, Fig. 2 shows an improvement in f_{in} and f_{ex} estimates for all models. The *coupled* (green) and *unconstrained* (red) models best estimate f_{in} with an error from 0.01 to 0.05 and variance under 0.08. The error of the model with *ground-truth* parameters remains stable, and the *fixed* model provides the worst estimations for most cases.

The true value of D_e also drives the estimates of D_i and D_e with the *coupled* and *unconstrained* models. Fig. 4 shows that the diffusion coefficient estimated by the *coupled* model (right) is close to D_e. When the optimization is *unconstrained* (left), D_i and D_e estimates are different but D_e estimates of *unconstrained* and *coupled* models are similar. Even with the *unconstrained* model, D_i estimations follow the trends of the true D_e (black triangle). Finally, the variance of D_e and D_i estimations respectively increases and decreases with D_e for both models. The estimated R is shown in Fig. 5. R estimates range from 2 to 4 μm. The *ground-truth* (cross) model provides a more stable estimation across (D_i, D_e) pairs and SNR (left). The center plot shows that the *unconstrained* model compensates the bad estimation of D_i by an overestimation of the cell radius (Center). Conversely, D_e has little influence on R.

Conclusion
Even if the substrates are designed to match the assumptions of the compartmentalized model, estimating the diffusion coefficients remains a challenging problem. Because R and Di have opposing effects on the signal, estimating both parameters is difficult. MCDS is a promising tool for studying the effect of tissue properties on DW-MRI signals. Future work will focus on testing new methods with MCDS to better disentangle model parameter estimation.

Acknowledgements
This work is partly supported by the Swiss National Science Foundation under grant Nbr 205320_175974. We acknowledge access to the facilities and expertise of the CIBM Center for Biomedical Imaging, a Swiss research center of excellence founded and supported by Lausanne University Hospital (CHUV), University of Lausanne (UNIL), Ecole polytechnique fédérale de Lausanne (EPFL), University of Geneva (UNIGE) and Geneva University Hospitals (HUG). Erick J. Canales-Rodríguez was supported by the Swiss National Science Foundation (SNSF, Ambizione grant PZ00P2_185814).

References
1. Rafael-Patino, J., Romascano, D., Ramirez-Manzanares, A., Canales-Rodríguez, E. J., Girard, G., & Thiran, J. P. (2020). Robust Monte-Carlo simulations in diffusion-MRI: Effect of the substrate complexity and parameter choice on the reproducibility of results. *Frontiers in neuroinformatics*, *14*, 8.
2. Lee, H. H., Fieremans, E., & Novikov, D. S. (2021). Realistic Microstructure Simulator (RMS): Monte Carlo simulations of diffusion in three-dimensional cell segmentations of microscopy images. *Journal of Neuroscience Methods*, *350*, 109018.
3. Panagiotaki, E., Walker-Samuel, S., Siow, B., Johnson, S. P., Rajkumar, V., Pedley, R. B., ... & Alexander, D. C. (2014). Noninvasive quantification of solid tumor microstructure using VERDICT MRI. *Cancer research*, *74*(7), 1902-1912.
4. Panagiotaki, E., Schneider, T., Siow, B., Hall, M. G., Lythgoe, M. F., & Alexander, D. C. (2012). Compartment models of the diffusion MR signal in brain white matter: a taxonomy and comparison. *Neuroimage*, *59*(3), 2241-2254.
5. Bonet-Carne, E., Johnston, E., Daducci, A., Jacobs, J. G., Freeman, A., Atkinson, D., ... & Panagiotaki, E. (2019). VERDICT-AMICO: Ultrafast fitting algorithm for non-invasive prostate microstructure characterization. *NMR in Biomedicine*, *32*(1), e4019.

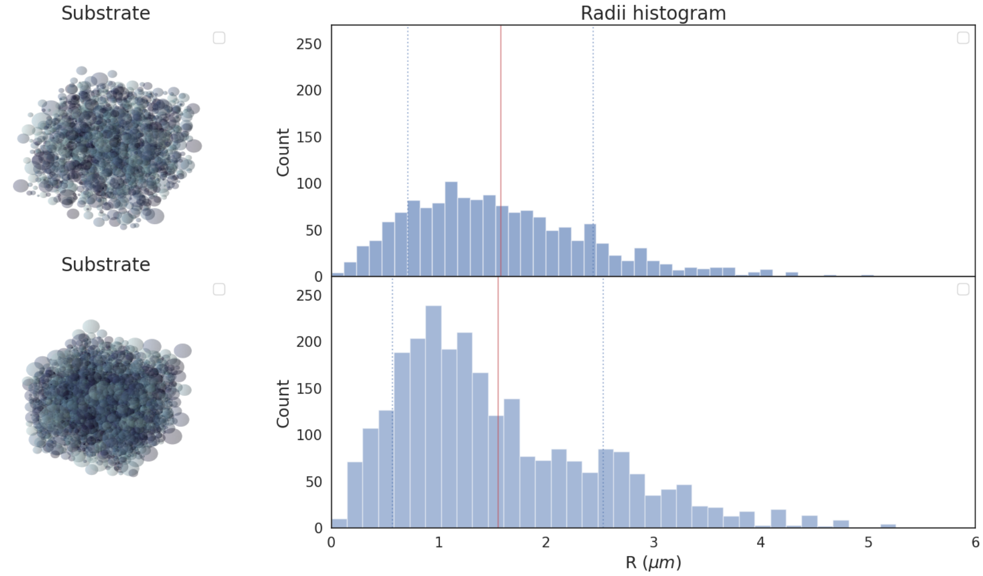

Figure 1: Examples of numerical substrates made of spheres for the MCDS (left column). Voxels are cubes of side length 70 μm with an ICVF of 0.3(top row) and 0.6 (bottom row). The radii of the spheres are sampled from a gamma distribution with a mean radius of 1.5 μm and a variance of 0.75 μm2 (right column).

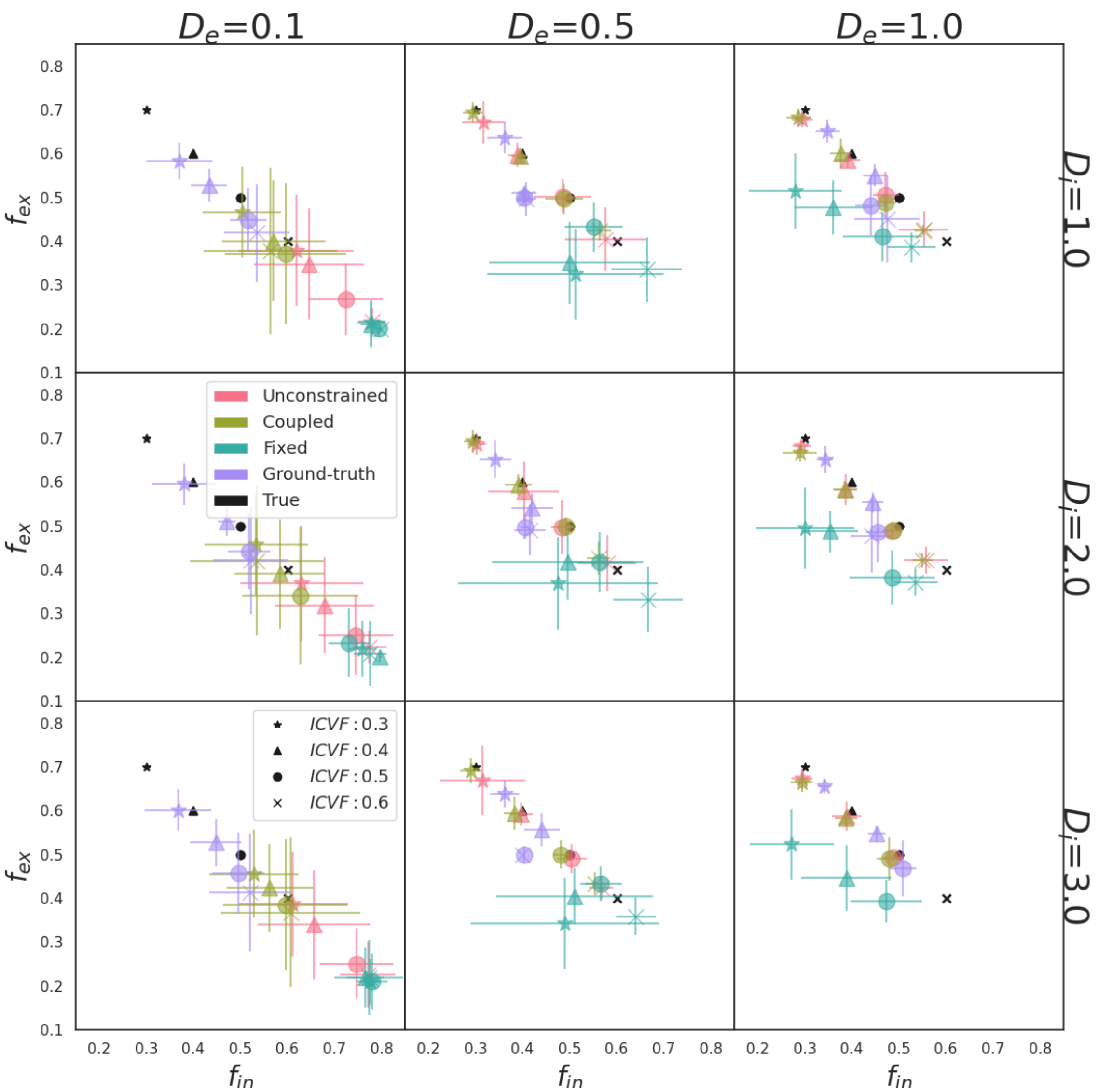

Figure 2: Scatter plots of f_in and f _ex estimations for all (D_i, D_e) μm²/ms pairs (subplot), all f_{in} (symbol) and all methods (colors) (SNR=20). Colored and black symbols are the results and the ground truth respectively. An overestimation of f_in or an overestimation of f_ex results in a colored symbol at the right or above the corresponding black symbols, respectively. Each symbol is located at the mean (f_in , fex) estimated from the 30 noisy signals, and the bars are the variance of the estimations.

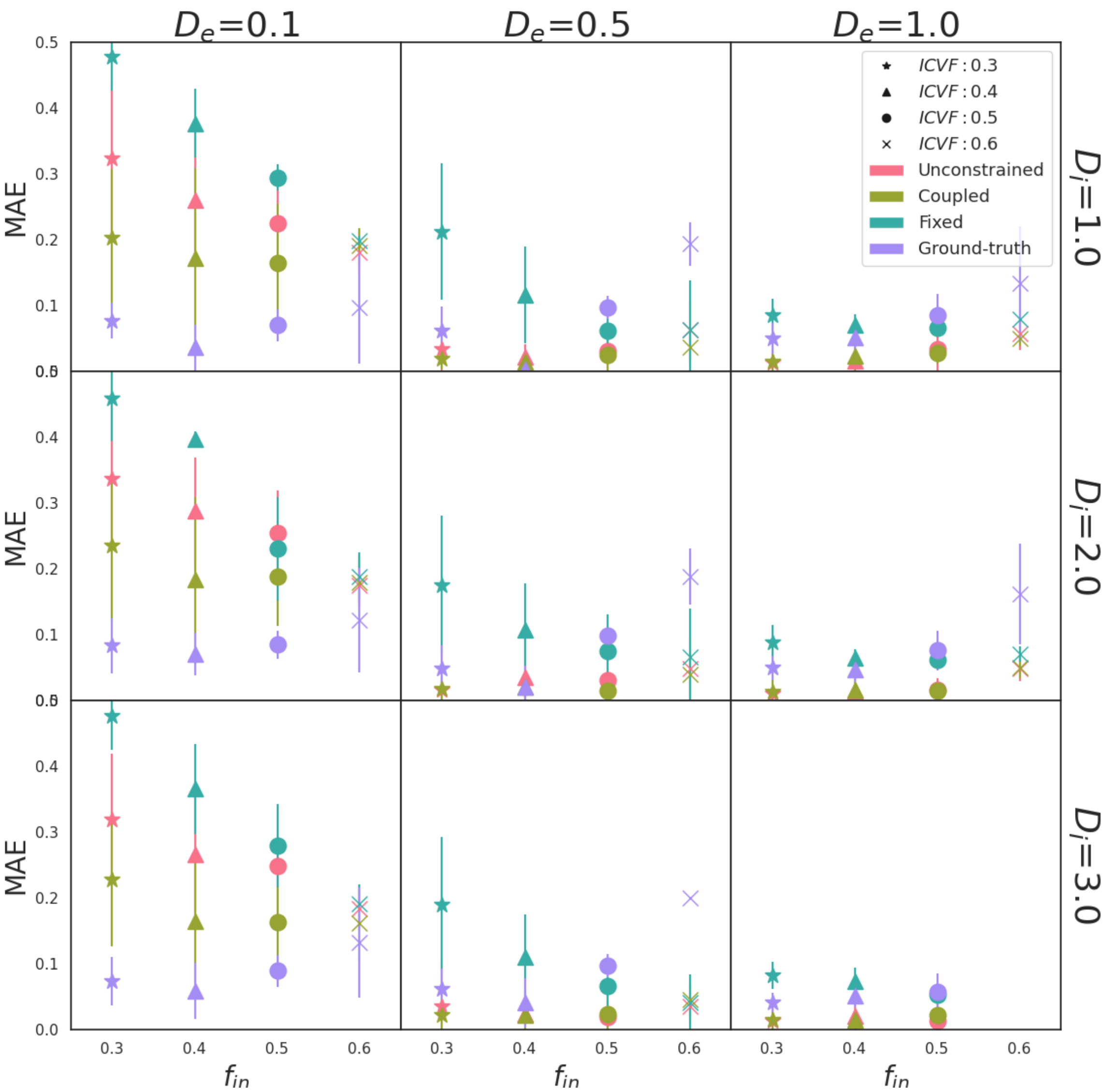

Figure 3: Mean absolute error (MAE) on the estimation of fin for all pairs (Di, De) μm²/ms(subplot), all fin(symbol) and all methods (color)(SNR= 20). Each symbol is located at the MAE on f_in estimated from the 30 noisy signals, and the bar is the corresponding variance of the error.

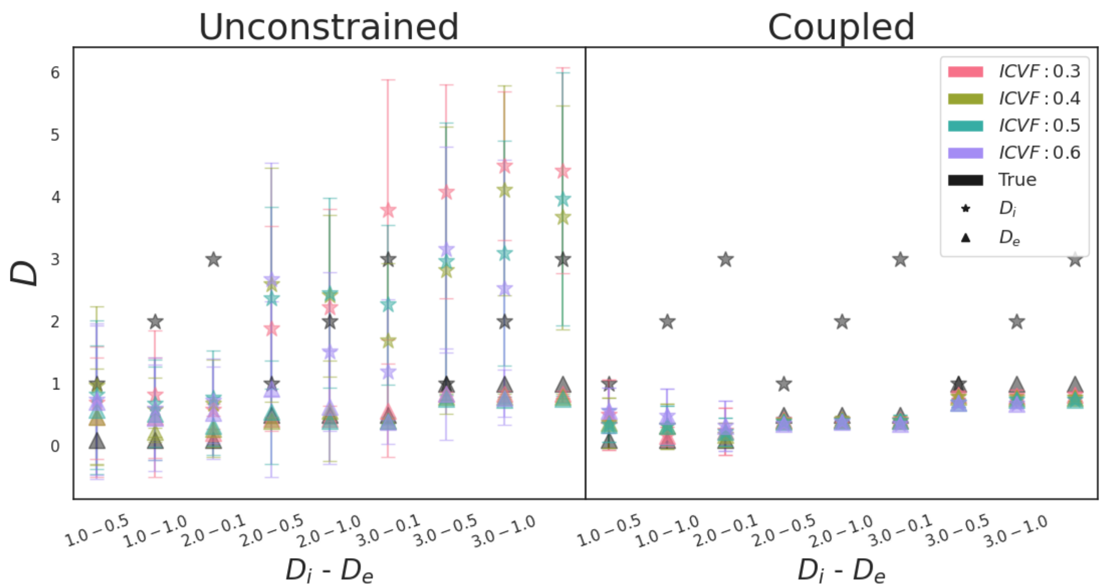

Figure 4: Estimation of D_i (star) μm²/ms and D_e (triangle) μm²/ms for the Unconstrained (left) and Coupled (right) model parameters for all f_in (SNR=20). Colored and black symbols are for the estimated and the true fin respectively. Each symbol is located at the mean estimation from the 30 noisy signals, and the bar is the variance of the estimations.

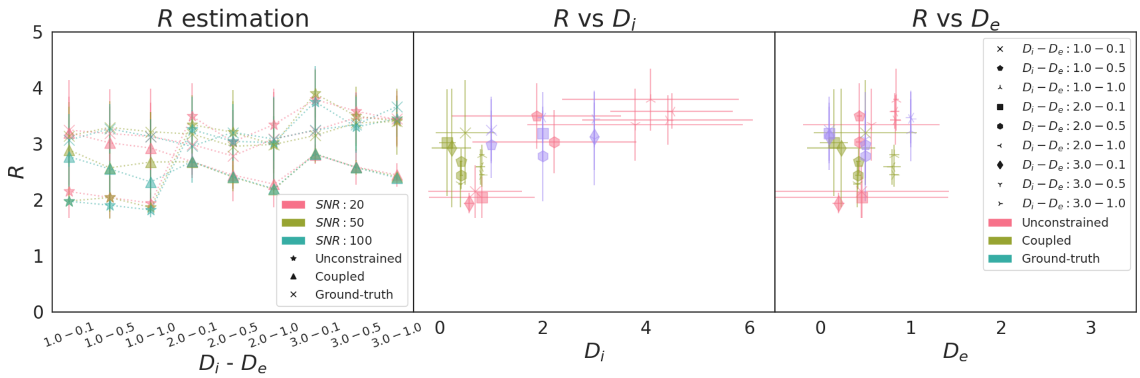

Figure 5 : Mean and standard deviation of the spheres' radii (R, μm) estimated by the Coupled (triangle) and the Unconstrained (star) models for all SNR (f_in = 0.6). Scatter plots of R with D_i (center) μm²/ms and D_e (right) μm²/ms estimated by the Coupled (green) and the Unconstrained (red) for all (D_i, D_e) μm²/ms pairs (SNR=20, f_in=0.6).